



Original articles

A practical algorithm for the design of multiple-sized porous scaffolds with triply periodic structures

Yibao Li ^a, Qing Xia ^a, Seungyoon Kang ^b, Soobin Kwak ^b, Junseok Kim ^{b,*}

^a School of Mathematics and Statistics, Xi'an Jiaotong University, Xi'an 710049, China

^b Department of Mathematics, Korea University, Seoul 02841, Republic of Korea



ARTICLE INFO

Keywords:

Triply periodic minimal surfaces
Porous scaffolds
Volume merging algorithm
Numerical design procedure
Implicit surfaces

ABSTRACT

In this study, we present a practical volume-merging method for generating multiple-sized porous structures that exhibit geometries with triply periodic minimal surface (TPMS) lattice structures. The proposed method consists of three stages: (1) designing the physical models with a signed distance field, (2) performing a merging operation for the porous scaffolds, and (3) assembling different units into a composite structure. The significant advantages of the proposed algorithm can be summarized as follows: Our method is independent of the model shape; the designed structures maintain a smooth surface with a constant mean curvature, and the mathematical computational complexity is low. We can join two different-sized triply periodic minimal surface lattices in the radial direction, where the transition region is obtained by smooth interpolation between the two lattice structures with different cell sizes or types. However, constructing large-sized models is only conceptually possible due to computational cost and memory storage constraints. To overcome these limitations, we present a practical method that can efficiently assemble large-scaled models at a low computational cost. The proposed method is based on a Boolean union operation of basic units of TPMS. Thus, it is simple to generate large-scale three-dimensional multiple-sized porous volumes based on our proposed method, which can be applied to many applications in mechanical and electrical engineering. The produced multi-scale compound scaffolds have smooth surfaces without fractures, making them suitable for straightforward application in additive manufacturing. Several numerical tests are conducted to validate the efficiency of the proposed algorithm.

1. Introduction

The exploration of porous scaffolds has garnered extensive attention in both science and industry due to its significance in a wide range of engineering applications. It plays a key role in tissue engineering [16,54,63], heat transfer using metal foams [3,39,48], flow in porous media [26,50], high permeability structures [4,34], and structure optimization in membrane distillation [14,40,52]. The cellular architectures designed by triply periodic minimal surfaces (TPMS) demonstrate a significant and consistent association with the target digital model [9,12]. Callens et al. [7] reviewed the response of cells and tissues to substrate curvature, providing a clear framework to describe cell and tissue-level curvature guidance. Three-dimensional porous scaffolds based on TPMS structures for bone tissue regeneration can be optimized to satisfy biological [47], mechanical, and mass transfer characteristics [5]. Zhanmanesh et al. [62] designed TPMS-based scaffolds for fluid permeability analysis. Qureshi et al. [36] demonstrated the excellent potential of

* Corresponding author.

E-mail addresses: yibaoli@xjtu.edu.cn (Y. Li), cfdkim@korea.ac.kr (J. Kim).

URLs: <http://gr.xjtu.edu.cn/web/yibaoli> (Y. Li), <https://mathematicians.korea.ac.kr/cfdkim/> (J. Kim).

TPMS-based phase change materials in latent thermal energy storage systems. Their results indicated a significant increase in thermal conductivity when TPMS-type cell structures were used, with the dominant impactors being the cell lattice type, their architectures, and porosity. While existing studies have successfully demonstrated the universality of TPMS lattice architectures, they have certain limitations concerning the following advantages: (i) the automatic control of physical indicators, such as volume fraction [10,42], structure and bulk pore size [55], and surface curvature [44]; (ii) the grading technique of cell size [2] and lattice type [58]; (iii) maximizing the transmission flux, such as energy absorption [41] and heat transfer [37]; and (iv) maintaining good fluid dynamic contexts, such as tortuosity [17,51], constant mean curvature [21,32], and permeability [8], while improving the lattice structure's strength.

TPMS lattices exhibit various features with controlled size and shape of the pores by varying manufacturing process parameters [49,61]. However, designing appropriate TPMS-based scaffolds remains challenging due to specific practical requirements [18]. Meanwhile, voxel-based [1] porous scaffolds should be combined with numerical algorithms [11], relaxing the freedom of choosing TPMS structures without losing adaptability. This technique of incorporating TPMS-based structural design into numerical algorithms is heuristic, attracting extensive attention to distinctive categories of integrated optimization algorithms. Fractal geometry plays key roles in biological and climatical modeling, representing complex geometric shapes that exhibit self-similarity across different scales. Saw and Chew [38] formulated the helicaliser using self-similar circular fractals, deriving the Hausdorff dimension for helicalised straight lines and circles. Perinelli et al. [33] studied the Takens estimator to characterize fractal geometry on a sphere, providing analysis regarding fractal geometries in seismology. Multi-scale topology optimization involves considering and optimizing structures at various resolutions or scales within a single design framework, aiming to achieve an optimal balance between global performance and local details. Garner et al. [15] presented a multiscale method for topology optimization of microstructures, including functionally graded materials and multiscale structures. Their method has been extended to comprehensively consider characteristics such as length gradient and isotropy, performing compound formulations for various physical problems such as conductivity and maximizing bulk modulus in a series of extensive studies [45,46]. Yu et al. [56] proposed a multiscale topology optimization method under the phase field framework, adopting a multi-regional microstructure composite design algorithm to balance the objective and various constraints. During their design process, the final distribution of TPMS-based microstructures maintained excellent physical properties for the macrostructure. A porous scaffold refers to a three-dimensional structure with voids or pores distributed throughout its volume, intentionally designed to allow the infiltration of fluids, cells, or other substances. Li et al. [25] proposed an approach that combines the TPMS-based algorithm and a random strategy to control the average pore size in the hexahedral mesh. By mapping the TPMS pores into the hexahedral mesh through a shape function, the porous scaffolds have more freedom and flexibility, making them useful for fabrication using additive manufacturing technologies. To combine computational features with the structure size of the unit TPMS structure and reduce the design complexity of porous scaffolds in the design process, we construct an efficient numerical approach that addresses the limitations of the theoretical design space.

Digital models in physical scenarios are composed of a large amount of data, typically consisting of triangles connected at the vertices [60]. For complex operating conditions, files with uniform specifications should be used. The challenge of combining multi-level design of digital models with limited storage space and simple computational operations has garnered particular attention in recent decades. Navangul et al. [30] developed an algorithm for selectively modifying stereolithography (STL) files to achieve the required tolerances specified on part features. In their design process, defective parts were eliminated to reduce material expenditure within the additive manufacturing framework. Zha and Anand [57] presented a numerical approach for densifying STL facets to virtually build the product with new patterns of facet formation. Their method can adaptively modify the corresponding triangles in an STL model without unnecessarily increasing storage requirements. To overcome the drawbacks of existing STL modifying strategies [35,53,59], our aim is to create an integrated approach based on a common type. This approach merges directly from a point cloud without additional overhead to complete the final block of our system.

In this paper, we present a practical volume-merging method for generating porous structures using triply periodic minimal surface (TPMS) lattice structures. This method is employed to determine the actual admissible design spaces with respect to adaptive interpolation. The proposed algorithm consists of three steps. The first step involves the design of the physical model using partial differential equation constraints. The second step is the merging operation with target structures, which can have different structure sizes, pore sizes, volume fractions, and lattice types. The third step involves combining the surface-only digital model with the designed porous scaffolds, achieved by the simple juxtaposition of vertices and oriented triangular meshes of the translated basic units. Boolean operations are applied before constructing the stereolithography format, obtained by creating total vertices and oriented triangular meshes in the stereolithography file format. This work aims to establish an integrated system, a practical extension of the work of Li et al. [24], where they proposed a TPMS-based volume-merging method. Our proposed method aligns with the logic of digital model by CAD design. This study addresses several issues: a designed procedure for arbitrary digital models has been developed to construct porous scaffolds with TPMS structures as the basic lattice. Our method is independent of the complex shapes of the target model. The compound structure obtained by the proposed method does not lose the characteristics of the TPMS. The proposed method has low computational complexity with less memory for storing the reconstruction of the surface mesh. Thus, it is simple to generate large-scale 3D porous volumes based on our method. The produced multiscale compound scaffolds have smooth surfaces with constant mean curvature, making them suitable for additive manufacturing. Compared to our previous studies [21,24], the novelties of the proposed model in this study can be summarized as follows: (i) This paper provides a solution for adaptive sizing design in lightweight porous scaffold for large-scale models. From the division of physical fields to the optimization of porous structures, and finally culminating in the establishment of the modified model, it constitutes a comprehensive and integrated process. (ii) The proposed method operates within a universal framework, not limited by physical properties such as TPMS structure types, sizes, and porosities. (iii) The formulation of the proposed method facilitates the maximization of structural

connectivity within the multi-scale framework while simultaneously ensuring consistent curvature. Various numerical simulations were presented to investigate the robustness of the proposed method.

This article is composed as follows. Section 2 introduces the signed distance field, triply periodic constant mean curvature surface structures and the combination strategy. Section 3 presents the numerical solution procedure of the porous scaffold design. In Section 4, we provide the numerical results at different stages of the total procedure to validate the efficiency of our algorithm. Finally, the concluding remarks and summaries of the proposed algorithm are given in Section 5.

2. Proposed algorithm

In this section, we expound upon the proposed approach by sequentially introducing the definition of signed distance fields, the methods for preserving constant curvature with different scales of unit structures, and the integration schemes between internal porous structures and shells. By using the physical field (symbolic distance field in this case), our solution enables adaptive partitioning of specified regions and filling them with porous structures of corresponding sizes and types. This process optimizes the curvature of composite structures, ensuring constant curvature characteristics while preserving structural connectivity. Furthermore, our method integrates shells and porous support structures, providing a comprehensive preparation for the direct implementation of additive manufacturing.

2.1. Signed distance field

Distance fields are widely used in industrial design and additional material manufacturing. A signed distance field contains internal characteristics of the model, through which we can control the manufacturing and designing accuracy, structural characteristics, and material properties at different distance levels. As shown in Fig. 1(b), we divide the whole domain into four sub-domains represented as white, cyan, green, and yellow. Let $\mathbf{x} \in \Omega$ and denote the closest point to \mathbf{x} by $\bar{\mathbf{X}}$ on $\partial\Omega$. Here Ω denotes the target three-dimensional model for which sign distance partitioning is to be performed. Let $\phi(\mathbf{x}) := s(\mathbf{x})\bar{d}(\mathbf{x})$ be a distance field, where $\bar{d}(\mathbf{x}) := \|\mathbf{x} - \bar{\mathbf{X}}\|$ and $s(\mathbf{x}) := \text{sign}((\mathbf{x} - \bar{\mathbf{X}}) \cdot \mathbf{N}(\bar{\mathbf{X}}))$, with an outward normal vector $\mathbf{N}(\bar{\mathbf{X}})$ at the boundary point $\bar{\mathbf{X}}$. We define the interior area as a positive value and the exterior zone is a negative value. $(\mathbf{x} - \bar{\mathbf{X}}) \cdot \mathbf{N}(\bar{\mathbf{X}})$ is the signed distance of \mathbf{x} to the tangent plane of $\bar{\mathbf{X}}$ as shown in Fig. 1(a). If $(\mathbf{x} - \bar{\mathbf{X}}) \cdot \mathbf{N}(\bar{\mathbf{X}}) \approx 0$, or $\mathbf{N}(\bar{\mathbf{X}})$ has noise, then $s(\mathbf{x})$ will also have noise. Therefore, we apply the following l_0 gradient regularization:

$$\min_s \sum_{\mathbf{x} \in \Omega} g(\mathbf{x}) \|\nabla s\|_0, \quad (1)$$

where $g(\mathbf{x}) = \tanh(\bar{d}(\mathbf{x})/(\sqrt{2}\xi))$ and ξ is a positive parameter. We need to elucidate the limitations of employing this approach for the segmentation of signed distance fields. This method exhibits constraints in its universal applicability when used on 2D and 3D objects characterized by continuous boundaries, particularly in scenarios where the objective is to partition such objects into distinct non-intersecting entities [23,43]. Challenges arise for complex closed surfaces with intricate geometries, primarily due to the potential existence of multiple intersections and the complexity of determining consistent signed distances. However, it is essential to note that the discontinuous symbolic distance field does not impede the application of our method to the lightweight scaffold design problem. In other words, even when employing symbolic distance-based segmentation to decompose a three-dimensional model into intersecting objects, our method remains capable of discerning and subsequently populating distinct unit structures of varying sizes [22].

2.2. The merging strategy for the triply periodic surface structures

TPMS is one of the significant structures that has been widely applied as lightweight scaffolds. TPMSs with constant mean curvature get extensive attention in materials, physics, mathematics, and biologies, as the geometry of TPMSs significantly affects the physical properties of the material [13,19,20,28,31]. Let us consider an example with the Schwarz P surface, which can be approximately generated from the following phase-field function:

$$\phi(x, y, z) = \cos(2\pi x) + \cos(2\pi y) + \cos(2\pi z), \quad (x, y, z) \in \Omega = [0, 1] \times [0, 1] \times [0, 1]. \quad (2)$$

The Schwarz P surface is obtained as an isosurface of $\phi(x, y, z) = c$, where c is a constant. Let us discretize the unit cubic domain Ω as

$$\Omega_h = \{(\mathbf{x}_i, \mathbf{y}_j, \mathbf{z}_k) | \mathbf{x}_i = h_x i, \mathbf{y}_j = h_y j, \mathbf{z}_k = h_z k, i \in \{0, 1, \dots, N_x\}, j \in \{0, 1, \dots, N_y\}, k \in \{0, 1, \dots, N_z\}\},$$

where $h_x = 1/N_x$, $h_y = 1/N_y$, and $h_z = 1/N_z$ denote the grid sizes along distinct axis directions. We will use $\phi_{ijk} = \phi(\mathbf{x}_i, \mathbf{y}_j, \mathbf{z}_k)$ for simplicity. As can be seen in Fig. 2(a), (b), and (c), the results are the isosurfaces of ϕ for $c = -0.5$, 0, and 0.5, respectively.

Let us consider the interpolating method for connecting two kinds of TPMS structures with different cell sizes [24], which will be illustrated using two Schwarz P surfaces as examples. We consider a larger P surface within the range $[0, 2] \times [0, 2] \times [1, 3]$, as shown in the top of Fig. 3(a) and four smaller P surfaces within the range $[0, 1] \times [0, 1] \times [0, 1]$, $[0, 1] \times [1, 2] \times [0, 1]$, $[1, 2] \times [0, 1] \times [0, 1]$, and $[1, 2] \times [1, 2] \times [0, 1]$, as shown in the bottom of Fig. 3(a). We extract the 0-level isosurface, which is computed from the volume data ϕ at the isosurface value 0, for the above five structures with different cell sizes. To smoothly merge these four small

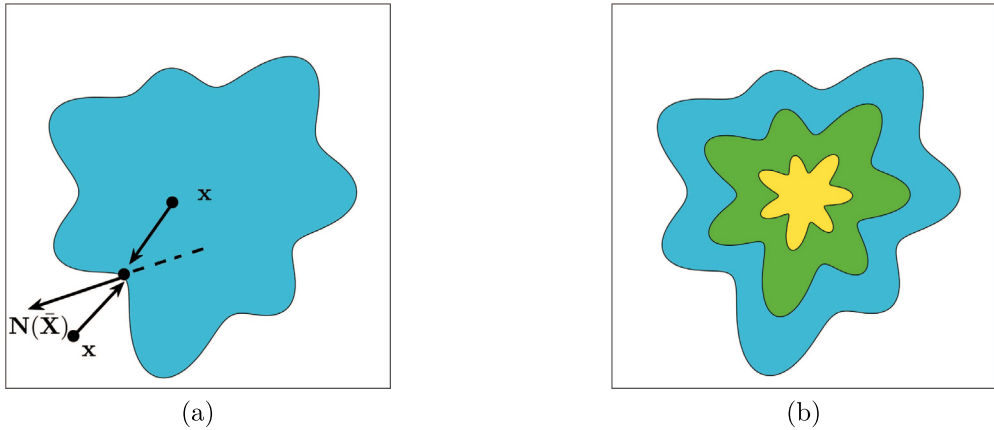


Fig. 1. Graphical explanation of signed distance field. (a) is the method to distinguish the external points and internal points of the model in the whole space. (b) is the contour figure. cyan, green and yellow represents the domain with signed distance [0.5 1], [0.25 0.5] and [0 0.25], respectively. (For interpretation of the references to color in this figure legend, the reader is referred to the web version of this article.)

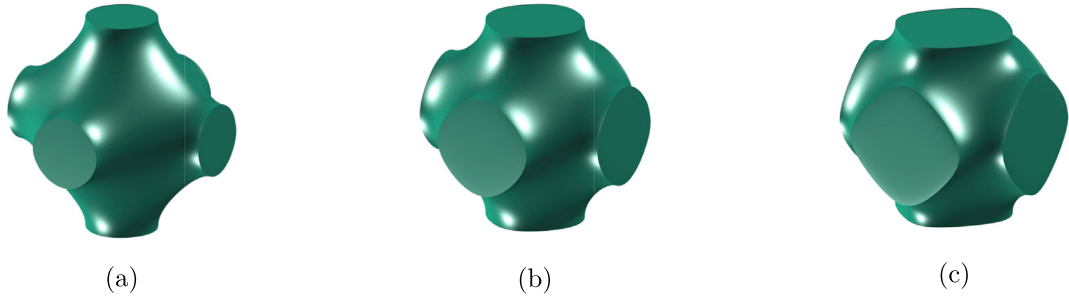


Fig. 2. (a), (b), and (c) are the isosurfaces of $\phi(x, y, z)$ for $c = -0.5, 0$, and 0.5 , respectively.

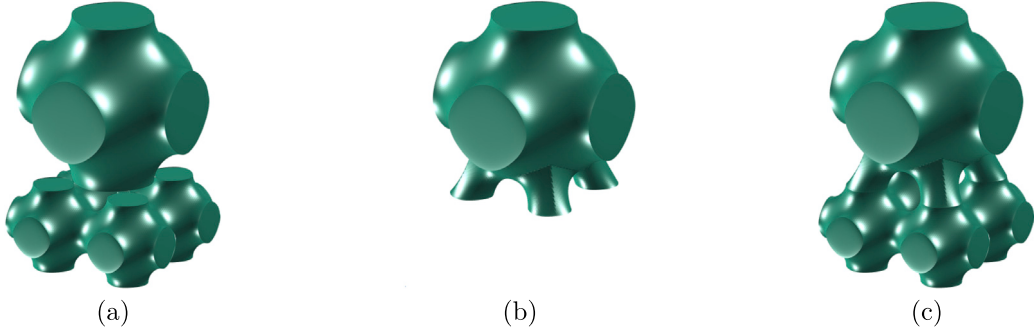


Fig. 3. Merging P surfaces of different size: (a) before merging, (b) after interpolation, and (c) merged structure.

bottom P surfaces with the larger top P surface, we modify a pyramid-shaped part of the larger P surface, as shown in Fig. 3(b). The merged structure is shown in Fig. 3(c).

To clearly explain the merging process of two differently sized P surfaces, we first consider the two-dimensional (2D) structures as counterparts of the three-dimensional procedure, as shown in Fig. 4. We uniformly discretize the domain, as shown in Fig. 4(a).

By using linear interpolation between a point value of the large P surface (represented by a circle \circ) and a point value of the smaller P surface (represented by a bullet \bullet), we can obtain the interpolated value on the bottom quarter part of the large P surface (represented by \times), as shown in Fig. 4(b). The shaded area in the figure is the filled contours of the phase-field function. We use the 2D schematic to illustrate the interpolation method, which can be directly extend to 3D space. A similar process is applied to the P surfaces in three-dimensional domain, as shown in Fig. 5. In Fig. 5(a), we illustrate the schematic discretization of the domain, where red circles represent the larger P surface area and blue dots represent the bottom smaller P surfaces. Fig. 5(b) shows

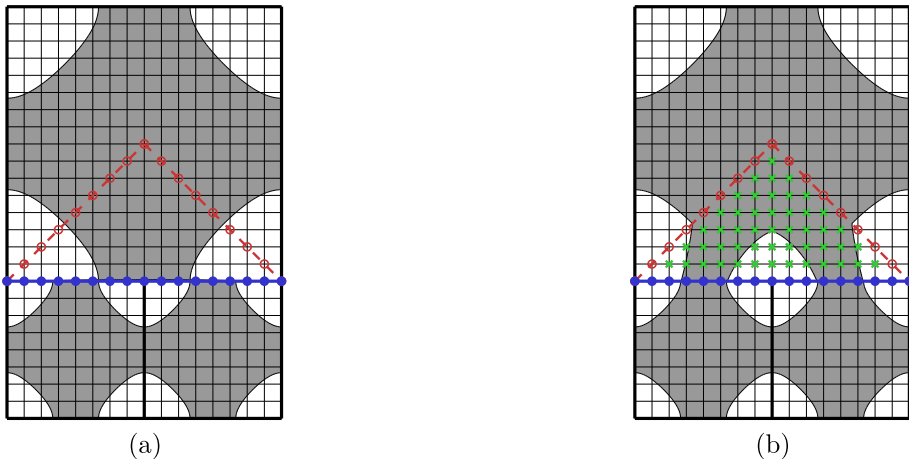


Fig. 4. Schematic illustration of merging two differently sized P surfaces: (a) before merging and (b) interpolation represented by \times from two points indicated by \circ and \bullet after merging process.

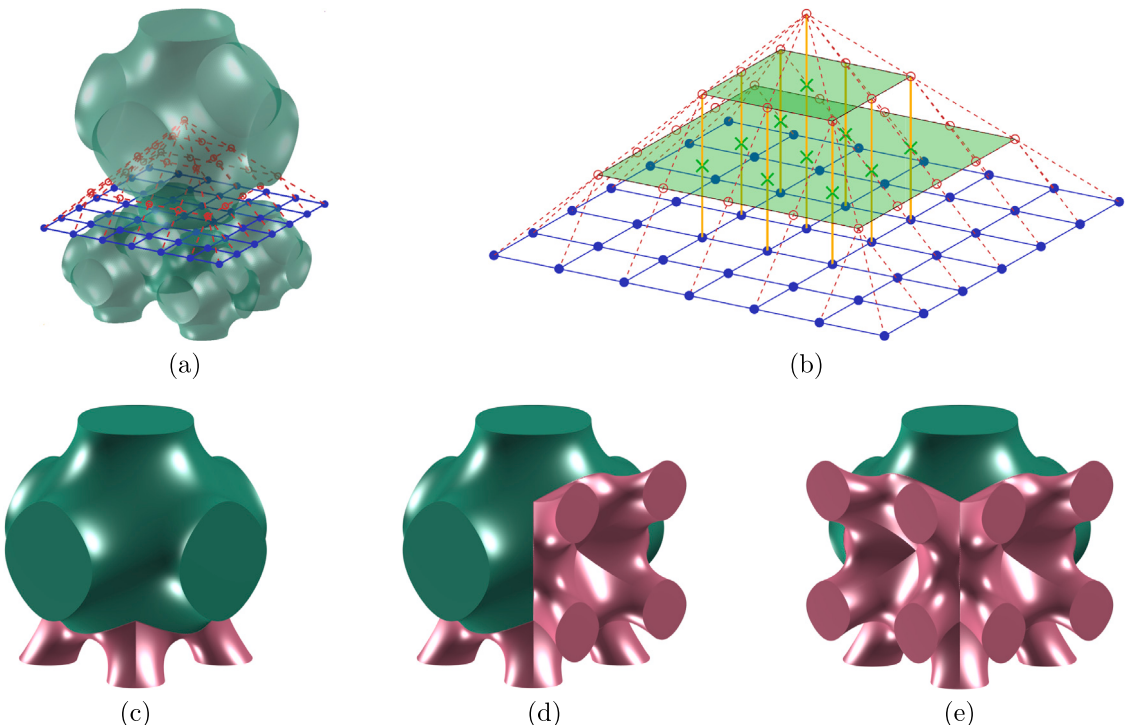


Fig. 5. Schematic of merging differently sized P surfaces in 3D domain: (a) discretization of a pyramid part of the larger P surface in 3D domain, (b) a magnified view of the interpolation region, (c) the interpolated result; (d) and (e) the results after modifying other one and two directional parts, respectively. (For interpretation of the references to color in this figure legend, the reader is referred to the web version of this article.)

a magnified view of the interpolation process, which is represented by the green (\times) symbol, and the interpolated result is shown in Fig. 5(c).

Fig. 5(d) and (e) show the results after modifying other one and two directional parts, respectively. It is worth emphasizing that our merging strategy is an interpolation-based method, which directly targets the point cloud and cannot guarantee the characteristic of constant mean curvature during the combination with different cell size TPMSSs. The merged structure should be polished under certain restrictive constraints to keep a constant mean curvature. To obtain a smooth surface, we used a modified Allen–Cahn

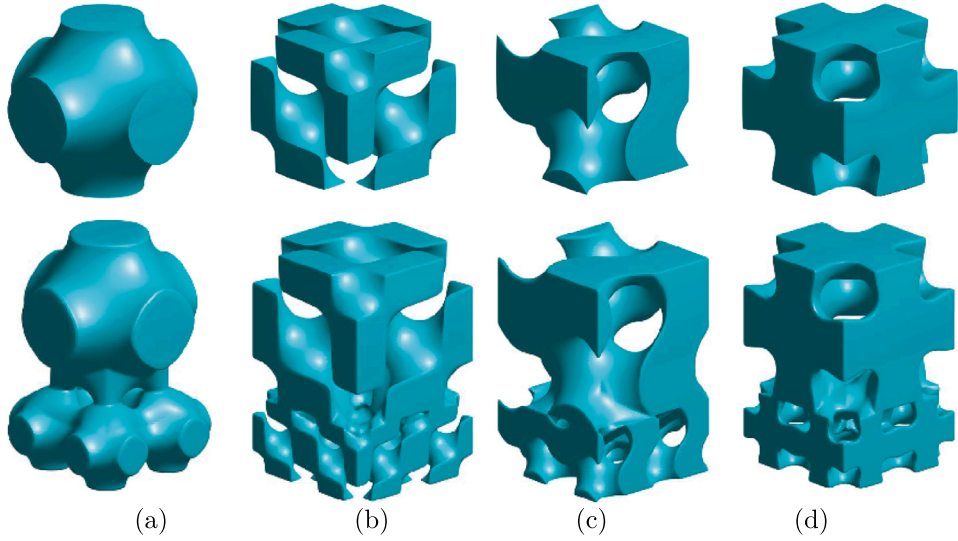


Fig. 6. Triply period minimal surfaces. (a) The Schwarz Primitive (P), (b) the Schwarz Diamond (D), (c) the Schwarz Gyroid (G), (d) the Schwarz I-WP (I) surface.

equation [21] as

$$\phi_t = -\frac{F'(\phi)}{\epsilon^2} + \Delta\phi + \lambda \frac{\phi(\phi - 1)}{\sqrt{2}\epsilon}, \quad (3)$$

where ϕ denotes the implicit surface $\Gamma = \{x : \phi(x) = 0.5\}$ in a 3D domain, $F(\phi) = 0.25\phi^2(1 - \phi)^2$ is the double-well potential and $\lambda = \sqrt{2} \int_{\Omega} F'(\phi) dx / [\epsilon \int_{\Omega} \phi(\phi - 1) dx]$. We should emphasize that the porous structure obtained thought this interpolation method is the initial solution of the Allen–Cahn equation. It is necessary to provide corresponding explanations for certain notations: ϵ is a positive parameter relates to the diffuse interface of small thickness, Δ is denoted as the Laplace–Beltrami operator and $\Delta\phi$ is used to delineate the diffusive impact of ϕ . To construct the triply periodic constant mean curvature surfaces, let the initial condition ϕ^0 as $\phi^0 = \alpha + \beta P$ by taking an example for P surface. For a given volume $V = \int_{\Omega} \phi^0 dx$, by taking integral of ϕ^0 , we can get $\alpha = (V - \beta \int_{\Omega} P dx) / \int_{\Omega} dx$. Because $\phi^0 \in [0, 1]$, we have $\alpha + \beta \max(P) \leq 1$ and $\alpha + \beta \min(P) \geq 0$. Thus, $\beta = \min((1 - \alpha)/\max(P), -\alpha/\min(P))$. There are also three other types of triply periodic minimal surfaces: the Schwarz Diamond (D), the Schwarz Gyroid (G), and the Schwarz I-WP (I) surfaces. These surfaces can also be the candidates for our merging strategy. It can be observed that we have generated the merged structures with constant mean curvature and smooth variation between different sized structures, which has a significant influence on the construction of multi-precision structure system. When considering the continuity properties of the modified model, it is necessary to note the following clarification: The merged composite structure after interpolation, as illustrated in Fig. 3, is only C^0 continuous. This implies that the structures involved share an identical position at the connection point. We achieve the property of curvature conservation for the composite structure by computing Eq. (3). The resulting modified structure, obtained through calculations with the interpolated composite structure as the initial values, exhibits C^2 continuity. As shown in the bottom row of Fig. 6, the continuous connections between structures with different sizes ensure the stability of our model. Furthermore, this method can adaptively change the porosity of the structure according to the actual demand to design the graded porous TPMS scaffolds.

2.3. Combination of two structure formats

When modeling TPMS structures in MATLAB, each surface data is saved in a structure format with two elements: vertices and faces, which represent the coordinates and oriented triangulation, respectively. Therefore, when combining two surface structures, we need to combine two structures into a single structure. Let V_1 and \mathcal{T}_1 be the coordinate matrix and triangulation matrix of the first surface structure, and V_2 and \mathcal{T}_2 be the coordinate matrix and triangulation matrix of the second surface. Assume each matrix is given as follows:

$$V_1 = [v_{1,1}, v_{1,2}, \dots, v_{1,p_1}], \quad \mathcal{T}_1 = [\Delta_{1,1}, \Delta_{1,2}, \dots, \Delta_{1,q_1}], \quad (4)$$

$$V_2 = [v_{2,1}, v_{2,2}, \dots, v_{2,p_2}], \quad \mathcal{T}_2 = [\Delta_{2,1}, \Delta_{2,2}, \dots, \Delta_{2,q_2}], \quad (5)$$

where $v_{i,j}$ is a 3×1 vector representing a point's coordinate and $\Delta_{i,j}$ is a 3×1 vector representing a triangulation face. The combined coordinate matrix V is obtained by simply augmenting V_2 after V_1 .

$$V = [v_1, v_2, \dots, v_{p_1}, v_{p_1+1}, \dots, v_{p_1+p_2}], \quad \text{where } v_i = \begin{cases} v_{1,i}, & \text{for } 1 \leq i \leq p_1, \\ v_{2,i-p_1}, & \text{for } p_1 + 1 \leq i \leq p_1 + p_2. \end{cases} \quad (6)$$

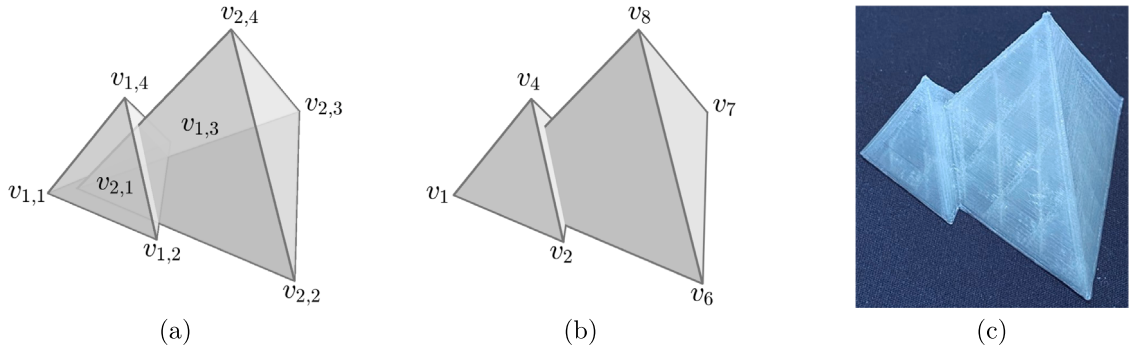


Fig. 7. (a) Before merging, (b) after merging, and (c) 3D printed model.

The combined triangulation matrix \mathcal{T} is obtained in a similar way using $\Delta' = \{p_1, p_1, p_1\}^T$, where p_1 is the number of points on the first surface. Adding Δ' to all elements of \mathcal{T}_2 and augmenting it after \mathcal{T}_1 results in

$$\mathcal{T} = [\Delta_1, \Delta_2, \dots, \Delta_{q_1}, \Delta_{q_1+1}, \dots, \Delta_{q_1+q_2}], \text{ where } \Delta_i = \begin{cases} \Delta_{1,i}, & \text{for } 1 \leq i \leq q_1, \\ \Delta_{2,i-q_1} + \Delta', & \text{for } q_1 + 1 \leq i \leq q_1 + q_2. \end{cases} \quad (7)$$

The following MATLAB function code is the core part of the combining algorithm, where input data consists of two surface structures, and the output data is the combined surface structure.

```
function ISO = sum_iso(iso1, iso2)
ISO.vertices = [iso1.vertices; iso2.vertices];
ISO.faces = [iso1.faces; iso2.faces+size(iso1.vertices,1)];
end
```

Let us consider a simple concrete example of merging two tetrahedrons. Assume we have a base surface with the coordinate matrix V_1 and an oriented triangulation matrix \mathcal{T}_1 as follows:

$$V_1 = \begin{bmatrix} -1.5 & 1.5 & 0 & 0 \\ -1 & -1 & 2 & 0 \\ 0 & 0 & 0 & 3 \end{bmatrix}, \quad \mathcal{T}_1 = \begin{bmatrix} 1 & 1 & 2 & 3 \\ 2 & 2 & 3 & 1 \\ 3 & 4 & 4 & 4 \end{bmatrix}. \quad (8)$$

The other base surface with the coordinate matrix V_2 and oriented triangulation matrix \mathcal{T}_2 are given as follows:

$$V_2 = \begin{bmatrix} 0 & 6 & 3 & 3 \\ 0 & 0 & 5 & 2 \\ 0 & 0 & 0 & 5 \end{bmatrix}, \quad \mathcal{T}_2 = \begin{bmatrix} 1 & 1 & 2 & 3 \\ 2 & 2 & 3 & 1 \\ 3 & 4 & 4 & 4 \end{bmatrix}. \quad (9)$$

Fig. 7(a) illustrates the two base tetrahedron structures. Applying the previously described merging algorithm, we get the combined coordinate matrix V and \mathcal{T} as

$$V = \begin{bmatrix} -1.5 & 1.5 & 0 & 0 & 0 & 6 & 3 & 3 \\ -1 & -1 & 2 & 0 & 0 & 0 & 5 & 2 \\ 0 & 0 & 0 & 3 & 0 & 0 & 0 & 5 \end{bmatrix}, \quad \mathcal{T} = \begin{bmatrix} 1 & 1 & 2 & 3 & 5 & 5 & 6 & 7 \\ 2 & 2 & 3 & 1 & 6 & 6 & 7 & 5 \\ 3 & 4 & 4 & 4 & 7 & 8 & 8 & 8 \end{bmatrix}, \quad (10)$$

which is shown in **Fig. 7(b)**. **Fig. 7(c)** shows the 3D printed model using a 3D printer. The same process can be applied to other complex surfaces.

We should point out that our method involves the direct concatenation of two matrices without considering issues related to facet intersection and coincidence. We employ this technique to integrate the internal porous structure of a three-dimensional model with the digitally represented surface, which is demonstrated in the subsequent sections, ultimately obtaining a comprehensive three-dimensional model. The integration technique described above is capable of satisfying this requirement. After the merged model is input into the 3D printer, it undergoes adaptive adjustments based on the requirements of slicing and G-code interpretation. This process includes Boolean intersection and difference operations to rectify the model into a closed three-dimensional structure, facilitating direct additive manufacturing. The discussion on coincidence and intersection issues in the concatenation process goes beyond the scope of this paper and could be explored in future research.

3. Methodology of our proposed algorithm

Our proposed method aims to generate models with adaptively designed lightweight scaffolds according to the corresponding physical fields. The input 3D model is voxelized, and the distances of the voxels on the outer surface are set to zero. If a voxel is

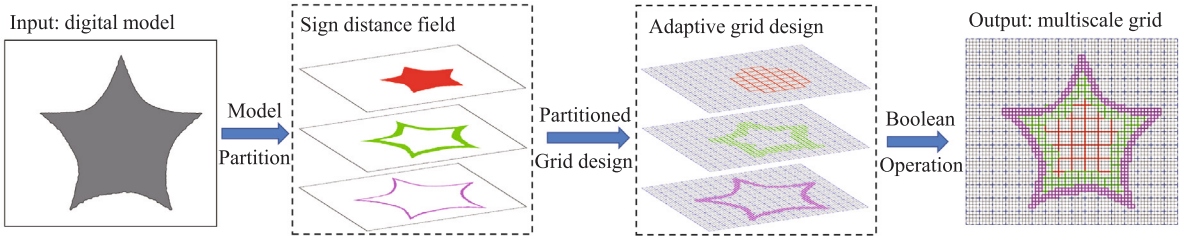


Fig. 8. Schematic for developing adaptive refinement mesh algorithm.

inside of the model, its distance is positive and it is calculated by using the minimal distance between the voxel on the boundary. Otherwise, if a voxel is outside the model, it will have a negative distance. The schematic for developing adaptive refinement mesh algorithm has been shown in Fig. 8. With the input digital model, we commence with sign distance partitioning. Subsequently, an adaptive grid design is employed, resulting in the generation of a comprehensive model featuring multiscale grids, predicated on the partitioning of distinct regions. The interval $[0, L]$ is partitioned into several sub-intervals or levels, where L is the largest positive distance. The voxels in each level are considered to be filled with the same accuracy. Here, the size of the voxel in each level should be specified. In order to illustrate the algorithm, we demonstrate the flowchart of the two-dimensional Star-model in Fig. 8. Let $\Omega = (0, L_x) \times (0, L_y) \times (0, L_z)$ be the 3D domain and we define $\phi_{i,j,k} = \phi((i-1)h + 0.5h, (j-1)h + 0.5h, (k-1)h + 0.5h)$. We introduce a hierarchy of increasingly finer grids, $\Omega_0, \Omega_1, \dots, \Omega_S$, restricted to subspaces with higher accuracy. Let $h_s = c \cdot h$ be the minimal length of domain Ω_s , where c is a positive integer. Then, the length of domain Ω_s is set as $h_s = 2^{S-s}h_S = 2^{S-s}c \cdot h$, for $s = 0, \dots, S$. Let $\hat{N}_x = N_x/(2^S c)$, $\hat{N}_y = N_y/(2^S c)$, $\hat{N}_z = N_z/(2^S c)$, where \hat{N}_x , \hat{N}_y , and \hat{N}_z represent the number of coarse mesh grids in each direction. Let d_s be the conditional thresholds, such as distance or stress values. For each small domain of the subspace Ω_s , we can count the number of points for which signed distance value is greater than d_s as follows:

$$\sum_{i=i_b}^{i_b+2^{S-s}c-1} \sum_{j=j_b}^{j_b+2^{S-s}c-1} \sum_{k=k_b}^{k_b+2^{S-s}c-1} f(\phi_{ijk}, d_s). \quad (11)$$

Here, $f(x, y) = 0$, if $x < y$, otherwise, $f(x, y) = 1$. In addition, i_b , j_b , and k_b are the indices of each small domain within the subspace Ω_s :

$$i_b = 1 + \sum_{m=0}^s (i_m - 1)2^{S-m}c, \quad j_b = 1 + \sum_{m=0}^s (j_m - 1)2^{S-m}c, \quad k_b = 1 + \sum_{m=0}^s (k_m - 1)2^{S-m}c,$$

where $\mathbf{i} = [i_0, i_1, \dots, i_s]$, $\mathbf{j} = [j_0, j_1, \dots, j_s]$ and $\mathbf{k} = [k_0, k_1, \dots, k_s]$ are three integer vectors. We refine the mesh grid based on the center point of every small domain. The center of Ω_s is defined as $C_x = (i_b - 1)h + 0.5h_s$, $C_y = (j_b - 1)h + 0.5h_s$, $C_z = (k_b - 1)h + 0.5h_s$. If the judgement condition is satisfied, we generate box elements with an accuracy of h_s in these subspaces. Otherwise, we divide the coarse space into eight fine subspaces and repeat the previous step. We divide the whole algorithm into the following steps.

- Step 1 : Calculate the location (C_x, C_y, C_z) of the central point in each box and generate the lightweight structure in the corresponding box.

- Step 2 : Refine the mesh grids under a judgement on whether to stratify according to the condition

$$\sum_{i=i_b}^{i_b+2^{S-s}c-1} \sum_{j=j_b}^{j_b+2^{S-s}c-1} \sum_{k=k_b}^{k_b+2^{S-s}c-1} f(\phi_{ijk}, d_s) = (2^{S-s}c)^3, \quad (12)$$

which determines whether the grid is fully immersed within the corresponding partitioned region. Upon updating the variable s and refining the next grid level for recursive computation, we exit the current loop and update (i_b, j_b, k_b) if the specified conditions are not met. The filtering space size can be selected adaptively with multiple printing sizes. By observing the output multiscale grid in Fig. 8, it is worth pointing out that our adaptive mesh algorithm can realize manufacturing with an arbitrary number of levels by considering the accuracy of 3D printer nozzles in engineering applications.

4. Application results and discussions

In this section, we focus on the numerical investigation of the intricate scaffold design, extensively exploring the entire procedure of designing porous scaffolds for the digital STL model based on unit porous structures. Initially, we conduct the voxel resolution simulation to determine the division of regions. Subsequently, we create porous scaffolds in a regular sphere model with Schwarz Primitive lattice of different structure sizes. To validate the universality of the proposed algorithm, we generate porous scaffolds in a more complex dragon model. Finally, we apply our method to topology optimization to show that the merging strategy can be employed in multiscale topology optimization with porous structure design.

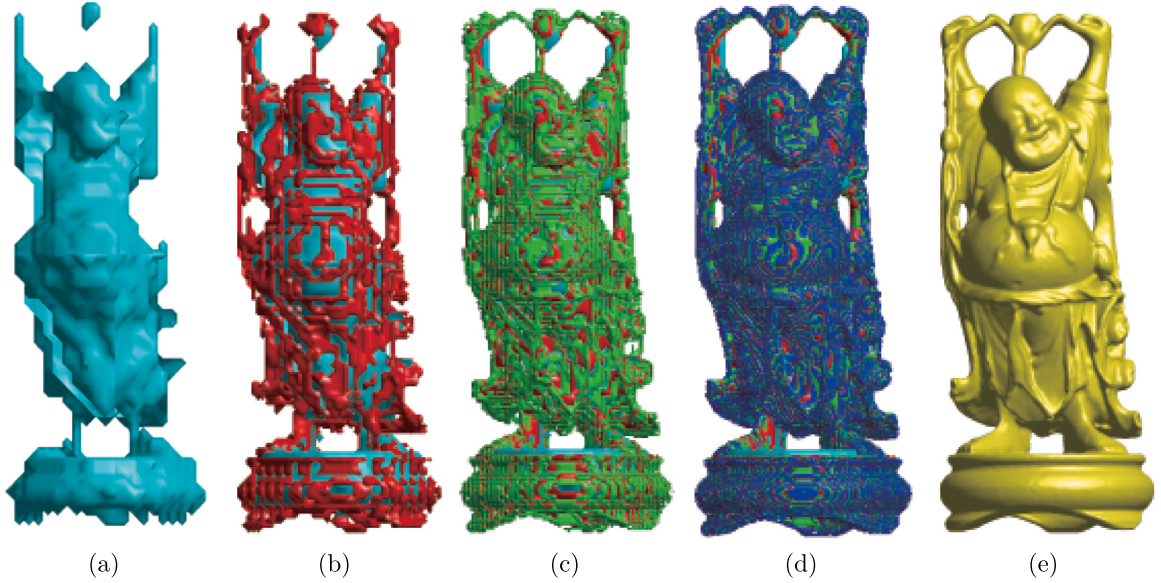


Fig. 9. Voxels combination process. From (a) to (e) shows the model construction process in which the size of unit voxel decreases and the spatial resolution increases layer by layer. cyan, red, green, blue and yellow to represent the areas filled with voxels of size 1, 2, 4, 8 and 16, respectively. (For interpretation of the references to color in this figure legend, the reader is referred to the web version of this article.)

4.1. Region partition based on the volumetric distance field

In this section, we present the process of a multiscale design method based on spatial resolution. The specific implementation in Fig. 9 shows the numerical results for 5 different sizes of voxels. The signed distance function is used here to partition the interior of the model, allowing for the placement of Triply Periodic Minimal Surface (TPMS) structures of different sizes within voxel partitions. Cyan, red, green, blue, and yellow represent areas filled with voxels of sizes 16, 8, 4, 2, and 1, respectively. It is important to emphasize that, due to the large size of the model, voxel features might not be clearly discernible in the segmented figures. However, as we progressively increase the resolution, expressing the model with smaller voxel units, the contours of the model gradually become clearer. Our method excels in seamlessly integrating spatial resolution with TPMS structure placement, ensuring a comprehensive and flexible design. Variable voxel sizes enable nuanced exploration of the interior, providing an efficient way to adapt TPMS structures to different scales. This adaptability enhances overall efficiency, establishing our approach as a robust tool for multiscale design based on spatial resolution.

4.2. Composite scaffold design in hemisphere

In this section, we present a composite scaffold for a hemisphere with different sized TPMS Schwarz P surfaces using the proposed method. First, we make a hemispherical shell with an outer radius of $R = 3$ and a thickness of $r = 0.5$. Here, the value of r is chosen to be larger than the diagonal of smaller P surface. The interior of the hemisphere is filled with P surfaces of sizes $2 \times 2 \times 2$ and $1 \times 1 \times 1$. Each P surface is placed so that its edges are on integer value points.

In addition, we densely pack P surfaces within the hemisphere to fill it completely without any gaps. Larger P surfaces of size $2 \times 2 \times 2$ are then placed within the interior of a hemisphere of radius 2. Subsequently, smaller P surfaces are positioned in the remaining space. When larger and smaller P surfaces come into contact, the proposed merging algorithm is applied to naturally merge the two different-sized P surfaces. Each added P surface is augmented to the previously existing surface structure to combine all surface structures. Fig. 10 demonstrates the composite scaffold obtained by using two Schwarz Primitive structures with different cell sizes. From left to right, the results of each stage of the proposed method are illustrated. Firstly, we show the merging results without a Boolean operation and a close-up view of the merged parts. According to the sphere size, we apply the Boolean operation on the designed porous scaffolds. Then, we show the top slice of the hemisphere. By combining the spherical shell and the merged scaffolds into one STL model, we obtain the final results, which can be directly used for additive manufacturing. Subsequently, we display the 3D printed model produced using the proposed method in different views, as shown in Fig. 11. From these results, it is evident that our method can generate a smooth transition between the unit lattices of multi-size units and can be directly applied to real additive manufacturing processes.

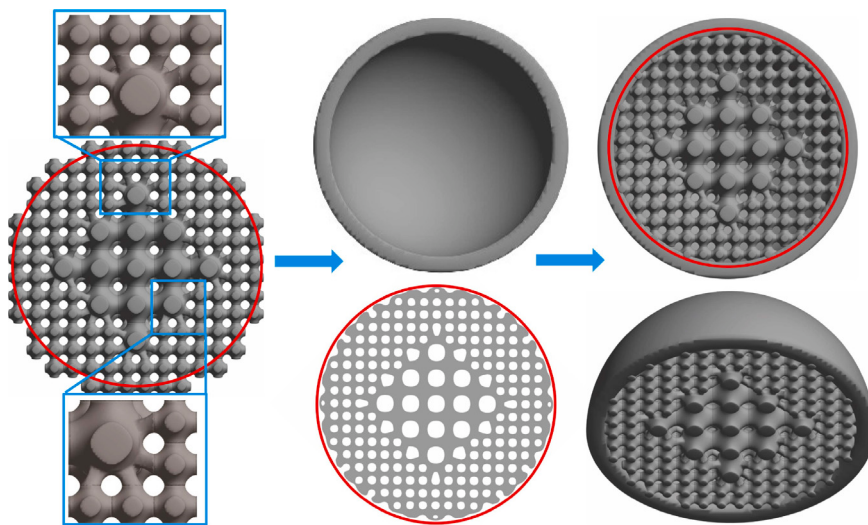


Fig. 10. Composite scaffold using two P surfaces of different sizes. From left to right, the simulations are the merging results without Boolean operation and the closed view of merging parts, the spherical shell with infinite thickness and the top slice of the hemisphere after Boolean operation, and the results using the proposed algorithm in different view angle, respectively.

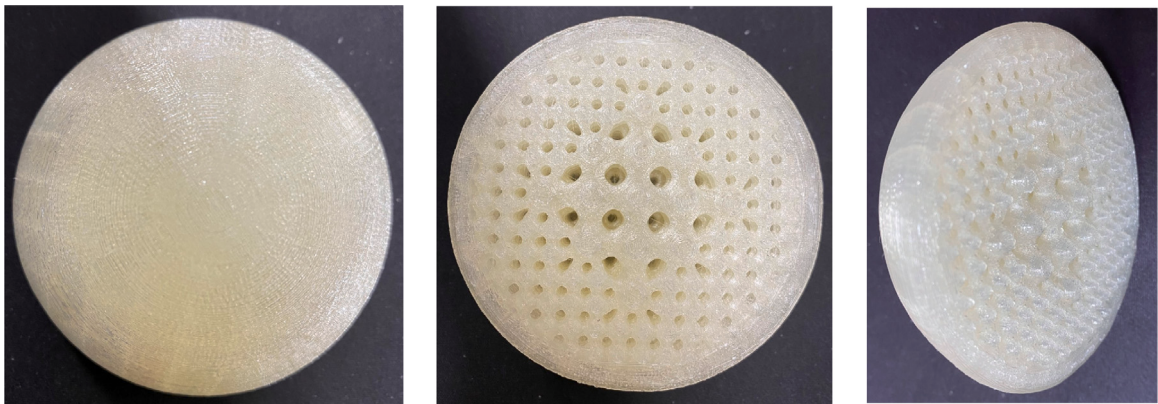


Fig. 11. Physical model manufactured from the proposed mathematical algorithm in different views.

4.3. Composite structure design with different type TPMS unit lattices

In this subsection, we perform our method in merging different types of TPMS units. Utilizing a variety of microscopic unit cells introduces a significant challenge, as neighboring volume elements often display either partial or complete mismatched characteristics. This mismatch can lead to design failures and render manufacturing impractical. Addressing these challenges requires the implementation of effective mitigation strategies, which have been systematically investigated in recent academic studies. Our consideration involves examining two adjacent cubic volumes and periodic TPMSs that share a common edge. As shown in Fig. 12(a), (b), and (c), we use Primitive-Gyroid, Primitive-Diamond, and Diamond-I-WP composite structures, respectively. The outcomes unequivocally demonstrate that our approach adeptly refines the surface of the composite structure while concurrently enhancing internal connectivity. Moreover, we illustrate curves to substantiate that the devised porous scaffold maintains the average mean curvature as shown in Fig. 12(d). From the results, we can observe that the average mean curvature increases and then converges to some value at the steady state. This demonstrates that our method can indeed modify the surface curvature of the merged model, achieving a state where the mean curvature is uniformly equal throughout, thereby satisfying the properties characteristic of minimal surfaces.

4.4. Porous scaffolds for the arbitrary STL model

To validate the universality of the proposed method, we perform the merging and combining strategies to an arbitrary STL model, which is the dragon model of the Stanford 3D scanning repository. According to the size of the dragon model, we divided the dragon

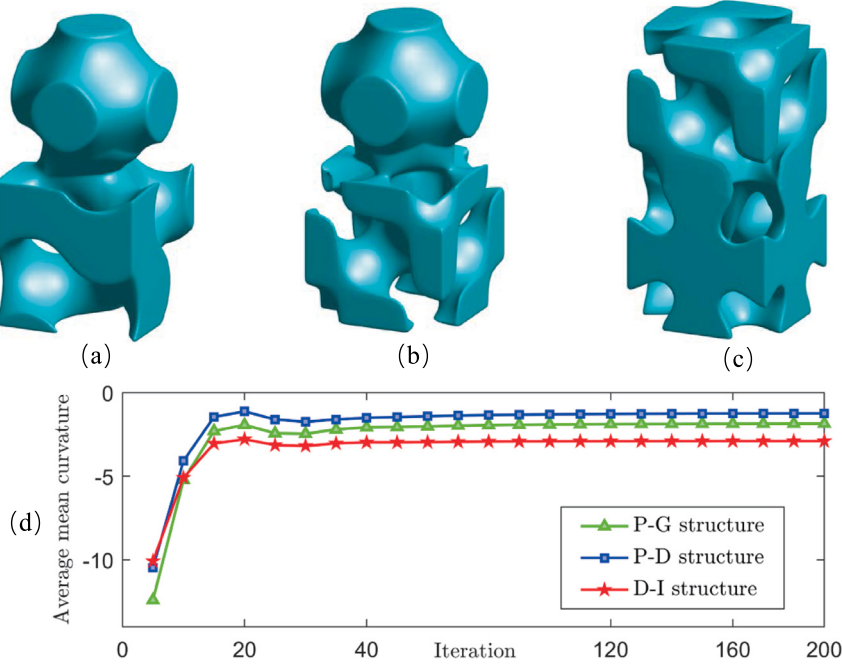


Fig. 12. Composite structures with different type of TPMS unit lattices. (a) is composed of Primitive and Gyroid structures. (b) is composed of Primitive and Diamond structures. (c) is composed of Diamond and I-WP structures. (d) is the evolution of the average mean curvature.

model into three layers, which are composed of different unit cells. As can be seen from Fig. 13(a) to (c), we demonstrate the internal three layers from 8 voxel resolution to 2 voxel resolution. According to the cell size of each layer, we replace the corresponding spacial voxels with the Schwarz Diamond lattices using our merging method. We should note that the Boolean operation has been applied to the surface layer, which is composed by 1 voxel resolution. As shown in Fig. 13(d), the porous scaffolds can be adaptively filled according to the voxel size. To avoid breakages on the model surface and prevent lightweight structures from exceeding the bounded surfaces, we performed boolean operations on the completed filling to ensure smoothness of the surface. By combining the surface of the digital model with the designed scaffolds, we obtained the final result as shown in Fig. 13(e). We realized the reconstruction of the digital model with lightweight scaffolds, which can be directly used in additive manufacturing. As can be seen from the results, our method can be used to achieve the merging of a shell and internal porous structure, which can be adaptively design to conserve the computational burden.

4.5. Coupling scheme with topology optimization

Topology optimization in the model, which solves a material distribution problem, is significant for generating an optimal topology in rapid prototyping [15,27]. In contrast to the traditional CAD method, the topology optimization method has more extensive and efficient design freedom [6].

According to the stress field, we can determine where materials or structures with a strong bearing capacity are needed and where less material can be used to reduce the weight of the model [29]. Before introducing the coupling scheme with topology optimization, we should present the objective of the topology optimization problem as follows:

$$\mathcal{J}(\phi, \mathbf{u}) = \int_{\Omega} W(\phi, \mathbf{u}) d\mathbf{x} = \int_{\Omega} \frac{1}{2} \mathcal{E}(\mathbf{u}) : \mathbf{D}(\phi) : \mathcal{E}(\mathbf{u}) d\mathbf{x}, \quad (13)$$

where ϕ is the optimal layout, \mathbf{u} is the displacement vector, \mathcal{E} is the strain tensor, and \mathbf{D} is the fourth-order stiffness tensor. By calculating the following linear elastic equations,

$$\mathcal{E}(\mathbf{u}) = \frac{1}{2} (\nabla \mathbf{u} + (\nabla \mathbf{u})^T), \quad \sigma(\phi, \mathbf{u}) = \mathbf{D}(\phi) : \mathcal{E}(\mathbf{u}), \quad \nabla \cdot \sigma(\phi, \mathbf{u}) = \mathbf{0}, \quad (14)$$

we aim to minimize the objective function, which represents the compliance of the cantilever beam structure. Here σ is a source-free stress tensor. The initial state of the substance is shown in Fig. 14(a), with a compliance calculated as 216.54. Fig. 14(b) can be obtained by fixing the left two corners of the rectangle and applying downward stress at the right center point. The compliance of the optimized structure is 145.11. Here, we assume the material to be a general anisotropic linear elastic material. Additionally, we can compute the stress distribution as shown in Fig. 14(c), where warmer colors represent larger stress values. As seen in the results, it is observed that stress is primarily concentrated at the intersection point in the middle of the cantilever beam. We refer to [56]



Fig. 13. Design results of the Stanford dragon, which has dimensions 95.4 mm × 68 mm × 44.4 mm. (a)–(c) Design results for each level. (d) The porous scaffold of the composite structure. (e) The combined results by merging of a shell (yellow part) and the internal porous structure. (For interpretation of the references to color in this figure legend, the reader is referred to the web version of this article.)

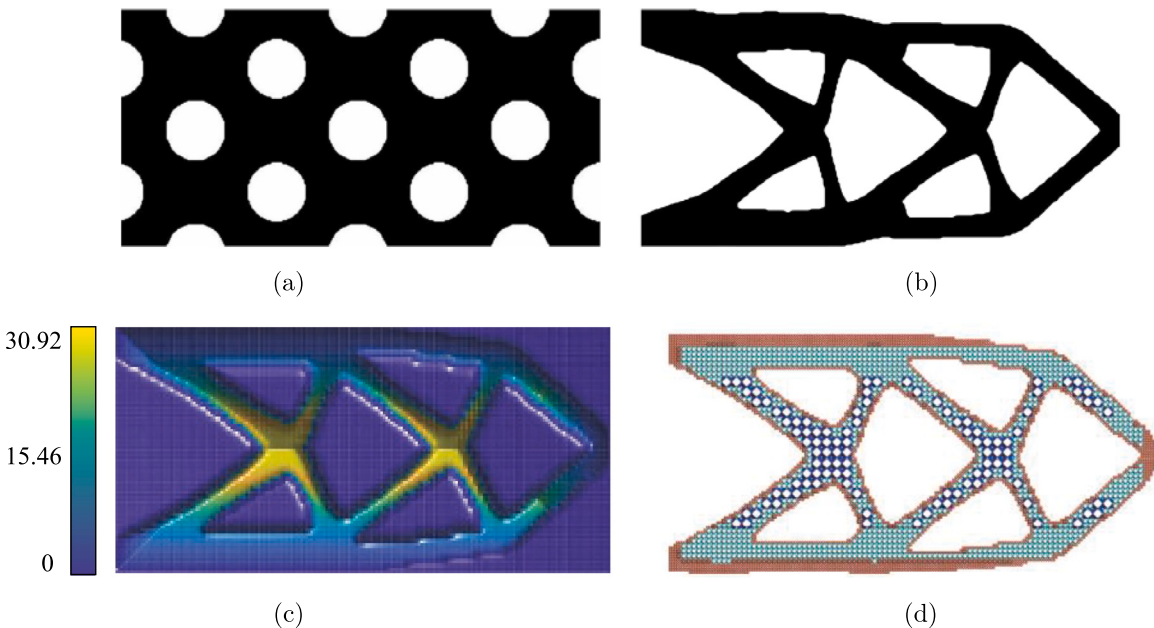


Fig. 14. Multiscale scaffolds implementation based on the stress distribution. (a) is the initial state. (b) is the result of topology optimization obtained by applying the downward force at the center point to the right of (a). (c) is the equipotential distribution of the stress field. (d) is multiscale scaffold with our adaptive algorithm from (c). Blue, cyan, and red represent the layers with voxel accuracies of 4, 2 and 1, respectively. (For interpretation of the references to color in this figure legend, the reader is referred to the web version of this article.)

Table 1

Lists of the number of levels, the actual model size, the time ratio R_T , the memory ratio R_M , and the CPU-times. Here $R_T = T_a/T_u$ and $R_M = M_a/M_u$, where T_a and M_a are the total time and memory with adaptive voxel size, T_u and M_u are the total time and memory with uniform voxel size.

Case	Layer size	Model size ((mm) ³)	R_T	R_M	CPU-time (s)
Fig. 9	5	44.8 × 105.6 × 44.8	7.18%	11.22%	249.05
Fig. 10	2	21.3 × 42.6 × 21.3	23.29%	68.16%	21.55
Fig. 13	4	95.4 × 68 × 44.4	1.46%	14.92%	318.92
Fig. 14	3	34.8 × 17.4 × 6.9	4.81%	26.76%	4.73

and couple our method with their multiscale topology optimization system. In Fig. 14(d), our proposed algorithm has shown good performance in the coupled computation and is well-adapted to the distribution of the stress field, guiding the merging relationship between TPMS-based lattice structures of different sizes. The compliance of the designed structure with a porous scaffold is 164.61. Two points need to be emphasized: (i) While the compliance of our porous structure is slightly greater than that of solid materials, our approach allows for substantial material savings without significantly compromising compliance. (ii) We compared the compliance of structures designed with a single-size porous configuration, yielding a compliance of 184.17, which is higher than that achieved through our adaptive methodology. Furthermore, our algorithm can easily divide the model into multiscale voxels, providing great convenience for subsequent lightweight scaffold design.

4.6. Computational performance test

In this subsection, we demonstrate the performance of all tests problem in this paper. Table 1 presents the information on the number of levels, the actual model size, the time ratio, the memory ratio and the CPU-times. Here the time ratio and the memory ratio are computed as $R_T = T_a/T_u$ and $R_M = M_a/M_u$, where T_a and M_a are the total time with adaptive voxel size, T_u and M_u are the total time with uniform voxel size. The CPU times (seconds) of our calculations are measured on 3.4 GHz with 8 GB of RAM. As can be seen from Table 1, the proposed algorithm in both the CPU-time and manufacturing time achieves high efficiency. Moreover, the utilization of our adaptive hierarchical algorithm can significantly reduce the memory consumption in storage. Compared to uniform designs, our approach is more suitable for large-scale computations. We can design different structures according to the different requirements in the internal area of the model. Furthermore, the use of multiple subspace partitions and multiple accuracy nozzles makes our algorithm more applicable.

5. Conclusion

In this article, we presented a practical volume merging method for generating porous structures using Triply Periodic Minimal Surface (TPMS) lattice structures. This method is versatile and can be easily applied to mechanics, electrical engineering, and tissue engineering. We constructed the design system in three steps: Firstly, we obtained the physical field in the actual model, which could come from external input or the solution of partial differential equations. Next, we applied the merging operation, which can integrate target structures, regardless of differences in size, porosity, or cell type. Finally, we combined the surface-only three-dimensional model with the designed porous structure, involving Boolean operations. The primary merits of the proposed algorithm can be summarized as follows: (1) It is not limited to complex shapes, and we can construct specific porous scaffolds with the given essential features. (2) The compound structures obtained by our method maintain properties of smooth surfaces, continuous gradient porosities, and constant mean curvature. (3) Our method does not require large memory storage for storing the compound structure and complex mathematical computation for the design of the merged porous scaffolds or the reconstruction of the surface mesh. Thus, it is simple to generate large-scale 3D porous volumes based on our method. The produced multiscale compound scaffolds have smooth surfaces with constant mean curvature, making them suitable for additive manufacturing. Various computational simulations were presented to investigate the robustness of the proposed algorithm.

CRediT authorship contribution statement

Yibao Li: Methodology, Software, Validation, Formal analysis, Investigation, Writing – original draft, Writing – review & editing, Supervision. **Qing Xia:** Software, Investigation, Data curation, Writing – original draft, Writing – review & editing, Visualization. **Seungyoon Kang:** Methodology, Software, Investigation, Resources, Data curation, Writing – original draft, Writing – review & editing, Visualization. **Soobin Kwak:** Validation, Investigation, Data curation, Writing – original draft, Writing – review & editing, Visualization. **Junseok Kim:** Conceptualization, Methodology, Validation, Formal analysis, Investigation, Resources, Writing – original draft, Writing – review & editing, Supervision, Project administration, Funding acquisition.

Declaration of competing interest

The authors declare that they have no known competing financial interests or personal relationships that could have appeared to influence the work reported in this paper.

Data availability

Data will be made available on request.

Acknowledgments

Y.B. Li is supported by National Natural Science Foundation of China (No. 12271430). The corresponding author (J.S. Kim) was supported by the BK21 FOUR program. The authors express their appreciation to the reviewers whose valuable insights and comments greatly enhanced the quality of this paper.

References

- [1] D. Abueidda, A. Dalaq, R. Al-Rub, H. Younes, Finite element predictions of effective multifunctional properties of interpenetrating phase composites with novel triply periodic solid shell architected reinforcements, *Int. J. Mech. Sci.* 92 (2015) 80–89.
- [2] M. Afshar, A. Pourkamali Anarak, H. Montazerian, J. Kadkhodapour, Additive manufacturing and mechanical characterization of graded porosity scaffolds designed based on triply periodic minimal surface architectures, *J. Mech. Behav. Biomed.* 62 (2016) 481–494.
- [3] S. Al-Omari, Z. Qureshi, E. Elnajjar, F. Mahmoud, A heat sink integrating fins within high thermal conductivity phase change material to cool high heat-flux heat sources, *Int. J. Therm. Sci.* 172 (2022) 107190.
- [4] R. Asbasi-Ghoudan, S. Galarreta, N. Rodriguez-Florez, Analytical model for the prediction of permeability of triply periodic minimal surfaces, *J. Mech. Behav. Biomed.* 124 (2021) 104804.
- [5] C. Bidan, K. Kommareddy, M. Rumpler, P. Kollmannsberger, P. Fratzl, J. Dunlop, Geometry as a factor for tissue growth: towards shape optimization of tissue engineering scaffolds, *Adv. Healthc. Mater.* 2 (2013) 186–194.
- [6] D. Brackett, I. Ashcroft, R. Hague, Topology optimization for additive manufacturing, in: Proceedings of the 24th Solid Freeform Fabrication Symposium, SFF'11, 2011, pp. 6–8.
- [7] S. Callens, R. Uyttendaele, L. Fratila-Apachitei, A. Zadpoor, Substrate curvature as a cue to guide spatiotemporal cell and tissue organization, *Biomaterials* 232 (2020) 119739.
- [8] A. Castro, T. Pires, J. Santos, B. Gouveia, P. Fernandes, Permeability versus design in TPMS scaffolds, *Materials* 12 (2019) 1313.
- [9] M. Centin, A. Signoroni, Advancing mesh completion for digital modeling and manufacturing, *Comput. Aided Geom. Des.* 62 (2018) 73–90.
- [10] J. Cheng, Q. Xia, J. Kim, Y. Li, An efficient linear and unconditionally stable numerical scheme for the phase field sintering model, *Commun. Nonlinear Sci. Numer. Simul.* 127 (2023) 107529.
- [11] D. Clarke, F. Dolamore, C. Fee, P. Galvosa, D. Holland, Investigation of flow through triply periodic minimal surface-structured porous media using MRI and CFD, *Chem. Eng. Sci.* 231 (2021) 116264.
- [12] J. Feng, J. Fu, C. Shang, Z. Lin, B. Li, Porous scaffold design by solid T-splines and triply periodic minimal surfaces, *Comput. Methods Appl. Mech. Engrg.* 336 (2018) 333–352.
- [13] S. Fujimori, M. Weber, Triply periodic minimal surfaces bounded by vertical symmetry planes, *Manuscripta Math.* 129 (2009) 29–53.
- [14] Yuliang Gao, Yujie Guo, Shijie Zheng, A NURBS-based finite cell method for structural topology optimization under geometric constraints, *Comput. Aided Geom. Des.* 72 (2019) 1–18.
- [15] E. Garner, H. Kolken, C. Wang, A. Zadpoor, J. Wu, Compatibility in microstructural optimization for additive manufacturing, *Addit. Manuf.* 26 (2019) 65–75.
- [16] A. Guerra, J. Belinha, R.N. Jorge, Using a meshless method to assess the effect of mechanical loading in angiogenesis, *Math. Comput. Simulation* 202 (2022) 421–441.
- [17] R. Guerreiro, T. Pires, J. Guedes, P. Fernandes, A. Castro, On the tortuosity of TPMS scaffolds for tissue engineering, *Symmetry* 12 (2020) 596.
- [18] F. Gunther, M. Wagner, S. Pilz, A. Gebert, M. Zimmermann, Design procedure for triply periodic minimal surface based biomimetic scaffolds, *J. Mech. Behav. Biomed.* 126 (2022) 104871.
- [19] Y. Hamza, H. Lin, Z. Li, Implicit progressive-iterative approximation for curve and surface reconstruction, *Comput. Aided Geom. Des.* 77 (2020) 101817.
- [20] J. Klinowski, A.L. Mackay, H. Terrones, Curved surfaces in chemical structure, *Philos. Trans. R. Soc. Lond. Ser. A Math. Phys. Eng. Sci.* 354 (1996) 1975–1987.
- [21] Y. Li, S. Guo, Triply periodic minimal surface using a modified Allen–Cahn equation, *Appl. Math. Comput.* 295 (2017) 84–94.
- [22] Y. Li, J. Kim, Fast and efficient narrow volume reconstruction from scattered data, *Pattern Recognit.* 48 (2015) 4057–4069.
- [23] H. Li, Y. Li, R. Yu, J. Sun, J. Kim, Surface reconstruction from unorganized points with L0 gradient minimization, *Comput. Vis. Image Underst.* 169 (2018) 108–118.
- [24] Y. Li, Q. Xia, S. Yoon, C. Lee, B. Lu, J. Kim, A simple and efficient volume merging method for triply periodic minimal structure, *Comput. Phys. Comm.* 264 (2021) 107956.
- [25] J. Li, Z. Xu, Q. Wang, G. Hu, Y. Wang, Coupling control of pore size and spatial distribution in bone scaffolds based on a random strategy for additive manufacturing, *Rapid Prototyp. J.* 256 (2019) 1030–1044.
- [26] T. Liu, Porosity reconstruction based on Biot elastic model of porous media by homotopy perturbation method, *Chaos Solitons Fractals* 158 (2022) 112007.
- [27] J. Liu, A. Gaynor, S. Chen, Z. Kang, K. Suresh, A. Takezawa, L. Li, J. Kato, J. Tang, C. Wang, L. Cheng, X. Liang, A. To, Current and future trends in topology optimization for additive manufacturing, *Struct. Multidiscip. Optim.* 57 (2018) 2457–2483.
- [28] E. Lord, A. Mackay, Periodic minimal surfaces of cubic symmetry, *Current Sci.* 85 (2003) 346–362.
- [29] Z. Luo, Y. Zhao, A survey of finite element analysis of temperature and thermal stress fields in powder bed fusion additive manufacturing, *Addit. Manuf.* 21 (2018) 318–332.
- [30] G. Navangul, R. Paul, S. Anand, Error minimization in layered manufacturing parts by stereolithography file modification using a vertex translation algorithm, *J. Manuf. Sci. Eng.* 135 (2013) 031006.
- [31] G. Nielson, K. Lee, L. Zhang, Lifting curve parameterization methods to isosurfaces, *Comput. Aided Geom. Des.* 21 (2004) 751–766.
- [32] L. Pagani, P.J. Scott, Curvature based sampling of curves and surfaces, *Comput. Aided Geom. Des.* 59 (2018) 32–48.
- [33] A. Perinelli, R. Iuppa, L. Ricci, Estimating the correlation dimension of a fractal on a sphere, *Chaos Solitons Fractals* 173 (2023) 113632.
- [34] T. Pires, J. Santos, R. Ruben, B. Gouveia, A. Castro, P. Fernandes, Numerical-experimental analysis of the permeability-porosity relationship in triply periodic minimal surfaces scaffolds, *J. Biomech.* 117 (2021) 110263.
- [35] Y. Qu, F. Wang, H. Fu, Stress analysis and thickness design of casting ceramics shells based on stereolithography prototypes, *Optoelectron. Adv. Mater.* 10 (2016) 91–96.
- [36] Z. Qureshi, S. Al-Omari, E. Elnajjar, O. Al-Ketan, R. Al-Rub, Using triply periodic minimal surfaces (TPMS)-based metal foams structures as skeleton for metal-foam-PCM composites for thermal energy storage and energy management applications, *Int. Commun. Heat Mass.* 124 (2021) 105265.

- [37] Z. Qureshi, S. Al-omari, E. Elnajjar, O. Al-Ketan, R. Al-Rub, On the effect of porosity and functional grading of 3D printable triply periodic minimal surface (TPMS) based architected lattices embedded with a phase change material, *Int. J. Heat Mass Transfer* 183 (2022) 122111.
- [38] V.L. Saw, L.Y. Chew, Helicalised fractals, *Chaos Solitons Fractals* 75 (2015) 191–203.
- [39] T. Tayebi, A.J. Chamkha, H.F. Öztop, L. Bouzeroura, Local thermal non-equilibrium (LTNE) effects on thermal-free convection in a nanofluid-saturated horizontal elliptical non-Darcian porous annulus, *Math. Comput. Simulation* 194 (2022) 124–140.
- [40] N. Thomas, N. Sreedhar, O. Al-Ketan, R. Rowshan, R. Al-Rub, H. Arafat, 3D printed spacers based on TPMS architectures for scaling control in membrane distillation, *J. Membr. Sci.* 581 (2019) 38–49.
- [41] Y. Tripathi, M. Shukla, A. Bhatt, Implicit-function-based design and additive manufacturing of triply periodic minimal surfaces scaffolds for bone tissue engineering, *J. Mater. Eng. Perform.* 28 (2019) 7445–7451.
- [42] S. Vijayaventaraman, L. Zhang, S. Zhang, J. Fuh, W. Lu, Triply periodic minimal surfaces sheet scaffolds for tissue engineering applications: an optimization approach toward biomimetic scaffold design, *ACS Appl. Bio. Mater.* 1 (2018) 259–269.
- [43] J. Wang, Y. Li, Y. Choi, C. Lee, J. Kim, Fast and accurate volume smoothing method using a modified Allen–Cahn equation, *Comput. Aided Des.* 120 (2019) 102804.
- [44] Y. Wang, X. Ren, Z. Chen, Y. Jiang, X. Cao, S. Fang, T. Zhao, Y. Li, D. Fang, Numerical and experimental studies on compressive behavior of gyroid lattice cylindrical shells, *Mater. Des.* 186 (2022) 108340.
- [45] J. Wu, O. Sigmund, J. Groen, Topology optimization of multi-scale structures: a review, *Struct. Multidiscip. Optim.* 63 (2021) 1455–1480.
- [46] J. Wu, C. Wang, X. Zhang, R. Westermann, Self-supporting rhombic infill structures for additive manufacturing, *Comput. Aided Des.* 80 (2016) 32–42.
- [47] Q. Xia, X. Jiang, Y. Li, A modified and efficient phase field model for the biological transport network, *J. Comput. Phys.* 488 (2023) 1112192.
- [48] Q. Xia, J. Kim, B. Xia, Y. Li, An unconditionally energy stable method for binary incompressible heat conductive fluids based on the phase–field model, *Comput. Math. Appl.* 123 (2022) 26–39.
- [49] Q. Xia, G. Sun, J. Kim, Y. Li, Multi-scale modeling and simulation of additive manufacturing based on fused deposition technique, *Phys. Fluids* 35 (2023) 034116.
- [50] Q. Xia, G. Sun, Q. Yu, J. Kim, Y. Li, Thermal-fluid topology optimization with unconditional energy stability and second-order accuracy via phase-field model, *Commun. Nonlinear Sci. Numer. Simul.* 116 (2023) 106782.
- [51] Q. Xia, J. Zhu, Q. Yu, J. Kim, Y. Li, Triply periodic minimal surfaces based topology optimization for the hydrodynamic and convective heat transfer, *Commun. Nonlinear Sci. Numer. Simul.* (2024).
- [52] W. Xie, Q. Xia, Q. Yu, Y. Li, An effective phase field method for topology optimization without the curvature effects, *Comput. Math. Appl.* 146 (2023) 200–212.
- [53] K. Xu, Y. Chen, Mask image planning for deformation control in projection-based stereolithography process, *J. Manuf. Sci. Eng.* 137 (2015) 031014.
- [54] Y. Yang, T. Xu, H. Bei, L. Zhang, C. Tang, M. Zhang, C. Xu, L. Bian, K. Yeung, J. Fuh, X. Zhao, Gaussian curvature-driven direction of cell fate toward osteogenesis with triply periodic minimal surface scaffolds, *Proc. Natl. Acad. Sci. USA* 119 (41) (2022) e2206684119.
- [55] D. Yoo, Computer-aided porous scaffold design for tissue engineering using triply periodic minimal surfaces, *Int. J. Precis. Eng. Manuf.* 12 (2011) 61–71.
- [56] Q. Yu, Q. Xia, Y. Li, A phase field-based systematic multiscale topology optimization method for porous structures design, *J. Comput. Phys.* 466 (2022) 111383.
- [57] W. Zha, S. Anand, Geometric approaches to input file modification for part quality improvement in additive manufacturing, *J. Manuf. Process.* 20 (2015) 165–477.
- [58] X. Zhang, G. Fang, L. Xing, W. Liu, J. Zhou, Effect of porosity variation strategy on the performance of functionally graded Ti-6Al-4V scaffolds for bone tissue engineering, *Mater. Des.* 157 (2018) 523–538.
- [59] Z. Zhang, S. Joshi, Slice data representation and format for multi-material objects for additive manufacturing processes, *Rapid Prototyp. J.* 23 (2017) 149–161.
- [60] G. Zhang, Y. Tsou, A. Rosenberger, Reconstruction of the homunculus skull using a combined scanning and stereolithography process, *Rapid Prototyp. J.* 6 (2000) 267–275.
- [61] X. Zhang, X. Yan, G. Fang, M. Liu, Biomechanical influence of structural variation strategies on functionally graded scaffolds constructed with triply periodic minimal surface, *Addit. Manuf.* 32 (2020) 101015.
- [62] M. Zhiamanesh, M. Varmazyar, H. Montazerian, Fluid permeability of graded porosity scaffolds architected with minimal surfaces, *ACS Biomater. Sci. Eng.* 5 (2019) 1228–1237.
- [63] S. Zou, Y. Mu, B. Pan, G. Li, L. Shao, J. Du, Y. Jin, Mechanical and biological properties of enhanced porous scaffolds based on triply periodic minimal surfaces, *Mater. Des.* 219 (2022) 110803.